Defense Threat Reduction Agency
8725 John J. Kingman Road, MS 6201
Fort Belvoir, VA 22060-6201

DTRA –TR- 06-18

Testing of Transient Radiation Noise Subtraction Using A Commercially Available 3-Color Visible Detector

TECHNICAL REPORT

January 2008

Kathryn L. Doughty and
Rudolf Goldflam

Prepared by:
ATK Mission Research
735 State Street
P.O. Box 719
Santa Barbara, CA 93101

20080213027

DESTRUCTION NOTICE

DISTRIBUTION LIST UPDATE

This mailer is provided to enable DTRA to maintain current distribution lists for reports. (We would appreciate you providing the requested information.)

- Add the individual listed to your distribution list.

- Delete the cited organization/individual.

- Change of address.

NAME: _____

ORGANIZATION: _____

OLD ADDRESS	NEW ADDRESS
_____	_____
_____	_____
_____	_____

TELEPHONE NUMBER: ( ) _____

DTRA PUBLICATION NUMBER/TITLE	CHANGES/DELETIONS/ADDITONS, etc.
	(Attach Sheet if more Space is Required)
_____	_____
_____	_____
_____	_____

DTRA or other GOVERNMENT CONTRACT NUMBER: _____

CERTIFICATION of NEED-TO-KNOW BY GOVERNMENT SPONSOR (if other than DTRA):

SPONSORING ORGANIZATION: _____

CONTRACTING OFFICER or REPRESENTATIVE: _____

SIGNATURE: _____

DEFENSE THREAT REDUCTION AGENCY
ATTN: CST
8725 John J Kingman Road, MS 6201
Fort Belvoir, VA 22060-6201

REPORT DOCUMENTATION PAGE

Public reporting burden for this collection of information is estimated to average 1 hour per response, including the time for reviewing instructions, searching existing data sources, gathering and maintaining the data needed, and completing and reviewing this collection of information. Send comments regarding this burden estimate or any other aspect of this collection of information, including suggestions for reducing this burden to Department of Defense, Washington Headquarters Services, Directorate for Information Operations and Reports (0704-0188), 1215 Jefferson Davis Highway, Suite 1204, Arlington, VA 22202-4302. Respondents should be aware that notwithstanding any other provision of law, no person shall be subject to any penalty for failing to comply with a collection of information if it does not display a currently valid OMB control number. **PLEASE DO NOT RETURN YOUR FORM TO THE ABOVE ADDRESS.**

1. REPORT DATE (DD-MM-YYYY)	2. REPORT TYPE	3. DATES COVERED (From - To)
00-12-2007	Technical	2/14/05 – 3/31/06

4. TITLE AND SUBTITLE

Testing of Transient Radiation Noise Subtraction using a Commercially Available 3-Color Visible Detector

5a. CONTRACT NUMBER	DTRA01-03-D-0004
5b. GRANT NUMBER	
5c. PROGRAM ELEMENT NUMBER	46AD

6. AUTHOR(S)

Kathryn L. Doughty, Rudolf Goldflam

5d. PROJECT NUMBER	BD
5e. TASK NUMBER	AA
5f. WORK UNIT NUMBER	09979

7. PERFORMING ORGANIZATION NAME(S) AND ADDRESS(ES)

ATK Mission Research
P. O. Drawer 719
Santa Barbara, CA 93102-0719

8. PERFORMING ORGANIZATION REPORT

MRC-R-1699

9. SPONSORING / MONITORING AGENCY NAME(S) AND ADDRESS(ES)

Defense Threat Reduction Agency
8725 John J. Kingman Rd., Stop 6201
Ft. Belvoir, VA 22060-6201
TDNR/RD/L. Palkuti

10. SPONSOR/MONITOR'S ACRONYM(S)

DTRA-TR-06-18

11. SPONSOR/MONITOR'S REPORT NUMBER(S)

12. DISTRIBUTION / AVAILABILITY STATEMENT

Approved for public release, distribution is unlimited.

13. SUPPLEMENTARY NOTES
This work was sponsored by the Defense Threat Reduction Agency under RDT&E RMC codes B 46A C K113 BD AA 09979.

14. ABSTRACT

Description of testing of commercial Foveon 3-color device for total dose radiation hardness as well as the technology's suitability for use of Self-Referential Transient Suppression (SRTS) radiation mitigation techniques. The detector was shown to be hard to 100KRads total ionizing dose. The results of tests as a radiation mitigation device showed excellent agreement with predictions and indicate that modification of the structure to optimize mitigation parameters will lead to a device that can perform in high radiation flux and fluence environments.

15. SUBJECT TERMS

Sensors	Fpas	Visible	Multispectral	Radiation Hard	Radiation Mitigation

16. SECURITY CLASSIFICATION OF:			17. LIMITATION OF ABSTRACT	18. NUMBER OF PAGES	19a. NAME OF RESPONSIBLE PERSON
a. REPORT UNCLASSIFIED	**b. ABSTRACT** UNCLASSIFIED	**c. THIS PAGE** UNCLASSIFIED		38	Kathryn Doughty **19b. TELEPHONE NUMBER** (include area code) 805-963-8761 ext 353

Standard Form 298 (Rev. 8-98)

Conversion Table

Conversion factors for U.S. Customary to metric (SI) units of measurement

MULTIPLY ———————————→ BY ———————————→ TO GET

TO GET ←——————————— BY ←——————————— DIVIDE

angstrom	$1.000000 \times E -10$	meters (m)
atmosphere (normal)	$1.01325 \times E +2$	kilo pascal (kPa)
bar	$1.000000 \times E +2$	kilo pascal (kPa)
barn	$1.000000 \times E -28$	meter^2 (m^2)
British thermal unit (thermochemical)	$1.054350 \times E +3$	joule (J)
calorie (thermochemical)	4.184000	joule (J)
cal (thermochemical) /cm^2	$4.184000 \times E -2$	mega joule/m^2 (MJ/m^2)
curie	$3.700000 \times E +1$	*giga becquerel (GBq)
degree (angle)	$1.745329 \times E -2$	radian (rad)
degree Fahrenheit	$t_K = (t_F + 459.67)/1.8$	degree kelvin (K)
electron volt	$1.60219 \times E -19$	joule (J)
erg	$1.000000 \times E -7$	joule (J)
erg/second	$1.000000 \times E -7$	watt (W)
foot	$3.048000 \times E -1$	meter (m)
foot-pound-force	1.355818	joule (J)
gallon (U.S. liquid)	$3.785412 \times E -3$	meter^3(m^3)
inch	$2.540000 \times E -2$	meter (m)
jerk	$1.000000 \times E +9$	joule (J)
joule/kilogram (J/kg) (radiation dose absorbed)	1.000000	Gray (Gy)
kilotons	4.183	terajoules
kip (1000 lbf)	$4.448222 \times E +3$	newton (N)
kip/inch^2 (ksi)	$6.894757 \times E +3$	kilo pascal (kPa)
ktap	$1.000000 \times E +2$	newton-second/m^2 (N-s/m^2)
micron	$1.000000 \times E -6$	meter (m)
mil	$2.540000 \times E -5$	meter (m)
mile (international)	$1.609344 \times E +3$	meter (m)
ounce	$2.834952 \times E -2$	kilogram (kg)
pound-force (lbs avoirdupois)	4.448222	newton (N)
pound-force inch	$1.129848 \times E -1$	newton-meter (N-m)
pound-force/inch	$1.751268 \times E +2$	newton/meter (N/m)
pound-force/foot^2	$4.788026 \times E -2$	kilo pascal (kPa)
pound-force/inch^2 (psi)	6.894757	kilo pascal (kPa)
pound-mass (lbm avoirdupois)	$4.535924 \times E -1$	kilogram (kg)
pound-mass-foot^2 (moment of inertia)	$4.214011 \times E -2$	kilogram-meter^2 (kg-m^2)
pound-mass/foot^3	$1.601846 \times E +1$	kilogram/meter^3(kg/m^3)
rad (radiation dose absorbed)	$1.000000 \times E -2$	**Gray(Gy)
roentgen	$2.579760 \times E -4$	coulomb/kilogram (C/kg)
shake	$1.000000 \times E -8$	second(s)
slug	$1.459390 \times E +1$	kilogram (kg)
torr (mm Hg, O° C)	$1.333220 \times E -1$	kilo pascal (kPa)

*The becquerel (Bq) is the SI unit of radioactivity; 1 Bq = 1 event/s.

**The Gray (Gy) is the SI unit of absorbed radiation.

Table Of Contents

Figures

Figures (Continued)

Section 1
Introduction

Many strategic, surveillance ad scientific sensors require high quality multicolor focal plane arrays that provide low noise performance and long mission life in presence of ionizing radiation. Three effects are of particular concern:

- Performance degradation due to total ionizing dose accumulated over mission life

- Performance loss due to accumulation of damage from heavy particle irradiation

- Radiation noise transients generated by β, p passing through the detector.

The first two effects are addressed generally by process control and readout circuit design. Typical hardness levels of interest are 100krad and 10^{11} n/cm^2. The last effect is a major concern affecting image quality. It is important whenever the ionizing radiation flux is such that more than 10% of pixels in any given image frame experience radiation events. Typically flux levels of $\sim 10^6$ β/cm^2/sec or 10^5 p/cm^2/sec are high enough to impact sensor performance so that off-FPA processing is inadequate for noise mitigation.

Various approaches to minimizing the magnitude of the radiation noise have been suggested. These are discussed later in this paper. In-detector based approaches are based on modification of detector architecture to either reduce the amplitude of the ionizing radiation pulse or use the detector to measure the pulse for immediate subtraction from the signal. The former approach as explored by us in previous series of tests consists of thinning the detector active volume to reduce the pulse amplitude. The approach works well in Schottky devices (reducing the amplitude of noise by a factor of 30). In Si detectors we demonstrated 8-fold pulse amplitude reduction but array manufacture suffers from nonuniformity issues. The second approach, referred here to as SRTS, uses an inactive detector layer to sense and measure the signal from radiation events and then subtract this from the optical signal in the active layer to eliminate noise.

The development of a commercial 3-color visible detector based on Foveon X3 technology presented an opportunity to model, test, and validate a new in-detector radiation mitigation approach, Self-Referential Transient Suppression (SRTS), without the high cost of developing a new detector. This paper describes the transient radiation mitigation technique explored and the evaluation of the SRTS approach using the Foveon X3 Pro device. We also present data on the total-dose radiation hardness of the device.

1.1 Foveon X3.

Foveon Inc. of Sunnyvale, California developed the Foveon X3 technology, leading to the creation of a visible detector with a new method of color separation. Unlike other multicolor

sensors which achieve 3 color sensitivity by providing three surface pixels per output pixel (mosaic capture), the Foveon pixel operates vertically (see Figure 1), using the innate difference in penetration depths of various wavelengths of visible light in silicon to separate the colors. A characteristic of this technology is the separate sensing of the charge built up in the layers of the pixel.
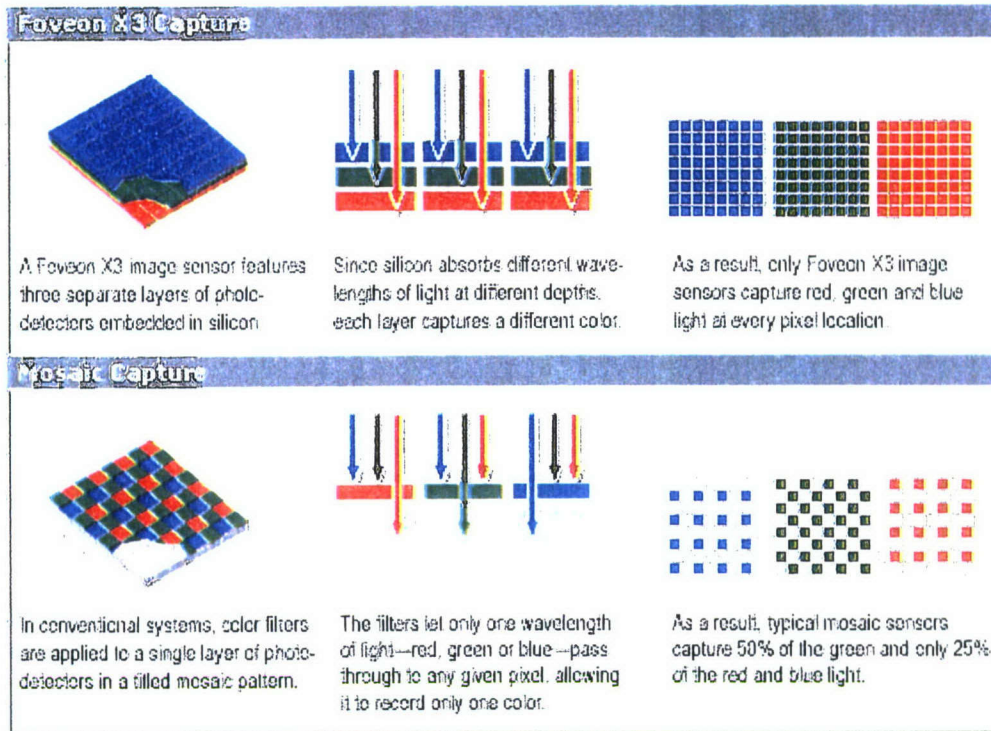

Foveon X3 Capture

A Foveon X3 image sensor features three separate layers of photo-detectors embedded in silicon.

Since silicon absorbs different wavelengths of light at different depths, each layer captures a different color.

As a result, only Foveon X3 image sensors capture red, green and blue light at every pixel location.

Mosaic Capture

In conventional systems, color filters are applied to a single layer of photo-detectors in a filled mosaic pattern.

The filters let only one wavelength of light—red, green or blue—pass through to any given pixel, allowing it to record only one color.

As a result, typical mosaic sensors capture 50% of the green and only 25% of the red and blue light.

Figure 1.   Foveon's X3 technology provides full fill-factor for all colors.

1.2   Transient Radiation Noise Suppression.

Using the Foveon device, ATK-MR investigated the transient radiation-induced noise suppression technique defined herein as Self-Referential Transient Suppression (SRTS). SRTS uses two detectors, both sensitive to radiation-induced transients, but only one being optically active. These are positioned in such a way that the expected radiation response to a given event is similar (in the case of the Foveon X3, the detectors are stacked vertically, see Figure 2.).

If both detectors sense the same transient radiation event, subtracting the signal of the optically inactive from the optically active detector will remove the radiation response and hence reduce the imager noise (see Figure 3).
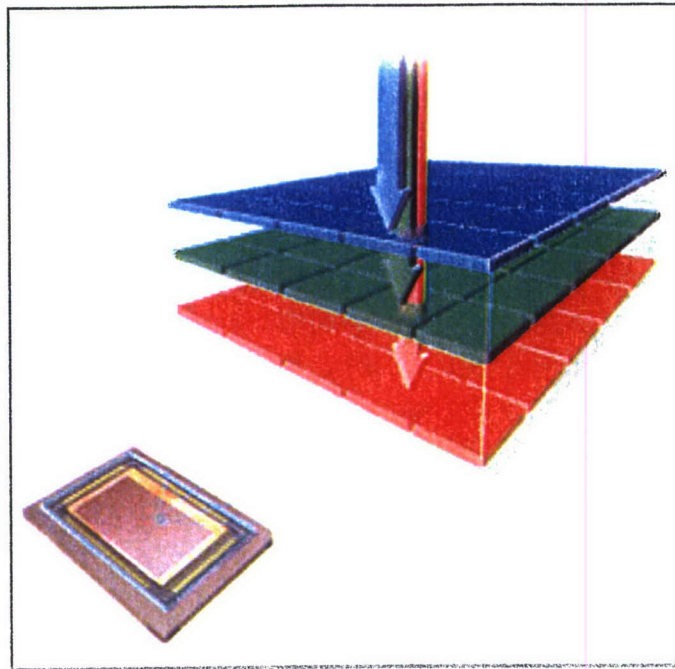
2
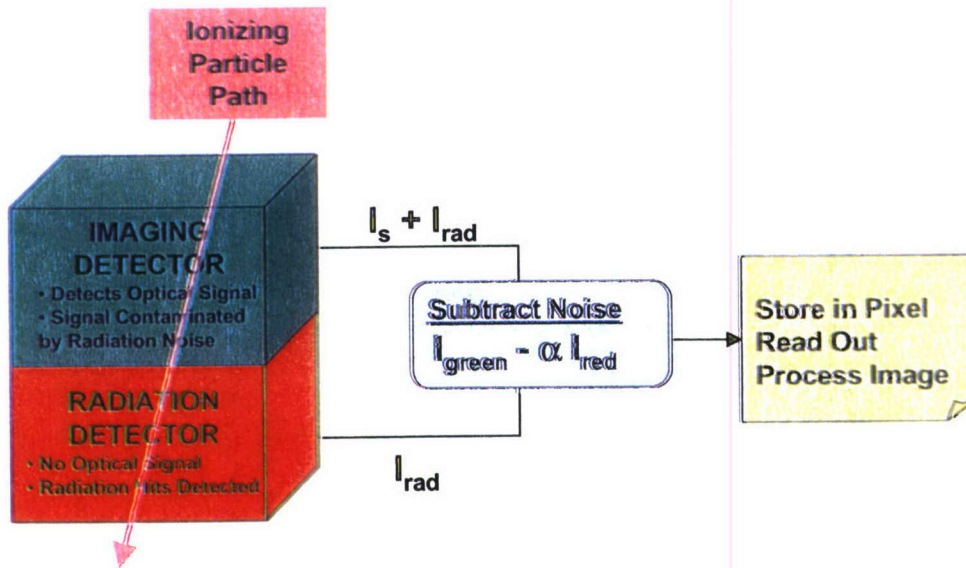
Figure 2.   The Foveon device.

Figure 3.   SRTS mitigation subtracts radiation noise from image signal.

SRTS was tested using the X3 by selecting one of the color layers as a radiation detecting (mitigating) layer. This layer is in very close proximity to the other two layers but with little

light input it thus plays the role of the optically inactive detector. The output from that color layer is used to mitigate the radiation noise in the other layers. The results of these tests are described in Section 3.

1.3   Radiation Hardness.

The Foveon X3 Pro array was also tested for radiation hardness. The array design is based on photo-diode detectors, which are much more radiation hard than CCDs. The associated circuitry is CMOS based, which has been seen to be more readily adapted to radiation environments than are other technologies. The array is a low noise, high dynamic range device. All of these factors made the Foveon X3 Pro an attractive sensor for testing for radiation environments. The results of our total dose degradation tests follow in Section 2.3.

A true rad-hard multi-color array that can also be implemented with transient radiation suppression could be valuable to the community as the basis for a hyperspectral sensor. Because of the high fill-factor achieved by the Foveon array, the sensitivity and resolution achievable are much higher than for comparable 3-color arrays. The Foveon design also lends itself to more accurate color registration, leading to better angular discrimination.

4

Section 2
Test Series

The test-series involved testing each of the layer's response to light, (as determined by appropriately chosen band-pass filters), as well as to ionizing radiation. This allowed us to determine the best band for use as the mitigating layer, and gave us information on the responses of the layers, and how they interact with each other (both physically, and in terms of any built-in processing circuitry). Total dose testing in this series was done with gammas. Proton and neutron testing should be performed later, as it seems warranted by our encouraging results.

The testing series included the following:

Measurement of optical response

The following optical measurements were made both pre-radiation, and at each level of irradiation during the total dose tests.

Dark Noise measurements as a function of integration time were made to determine:

- Dark Current

- Dark Current Fixed Pattern Noise.

Dark Frame (i.e. no light) measurements were made to determine:

- Read Fixed Pattern Noise

- Mean Dark Offset.

For the pre-radiation tests, responsivity curves were produced for each detector layer, using band-pass filters to select the stimulating light wavelength. Stimulating wavelength was varied by 50nm increments across the detector's sensitive waveband (from 405 to 660 nm). This demonstrated the variation in band response as a function of wavelength.

Bright Field Parameters were determined from the responsivity curve, allowing the evaluation of quantum yield, well capacity, linearity, sensitivity, signal-to-noise, and dynamic range for the device.

For the Total Dose tests, a single wavelength (550nm) light source was chosen for determining the Bright Field Parameters. 550nm light was chosen as it simulated all three detector bands with approximately the same efficiency (Figure 6). Data can thus be acquired for all layers simultaneously.

Total dose testing

Total Ionizing Dose (TID) testing up to 100 kRad(Si) was performed to determine the TID radiation hardness of the device. Optical response characteristics were measured at logarithmically spaced TID values.

Measurement of transient radiation response

- Measurements of the transient radiation response of each layer due to gamma-generated Compton betas were made. Event rates in the 0 to 6 events/read range were used.

- Low event rate data (< 0.1 events/read) were taken to provide statistics of the pulse height distribution curves for the individual layers as well as for the device as a whole.

- The distribution of the ratios of the pulse heights generated in each layer of the pixel relative to the others was derived in order to determine the best way to correlate the radiation transient signal generated in the individual layers, and how to best remove the resultant noise pulse. This approach also measured the degree of "mis-fit" between the layer responses, which we anticipate to be the ultimate limit on the efficacy of this mitigation method.

2.1 Description Of Test Series.

The only physical test-beds required were for optical characterization and gamma radiation testing. Both of these are readily available at ATK-MR's Longmire Lab, using their 870 Ci ^{137}Cs source and optical equipment which includes a calibrated Labsphere visible source and Spectra Physics power meters, as well as the necessary optics. ATK-MR maintains a suit of data analysis tools capable of handling the large data-sets necessary for the described analysis. A picture of the test-bed is shown in Figure 4.
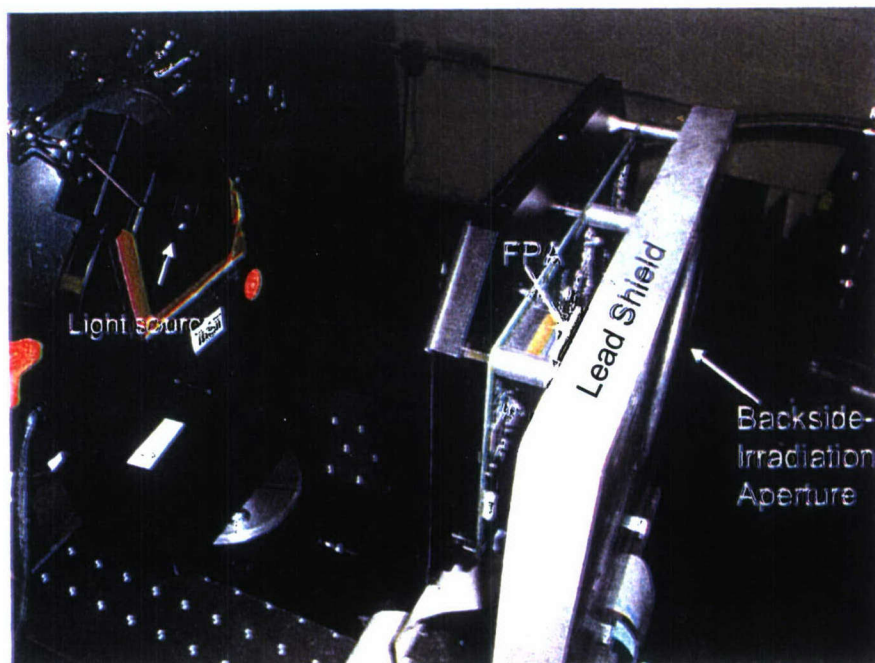

Figure 4. Test set-up.

6

A summary of the tests performed along with the derivable data products is shown in Table 1. A discussion of the test series follows.

Table 1.   Summary of test series.

Test	Test type	Justification	Data Product	Light	Radiation
Dark Current as Function of Integration Time	Optical-Dark	Determine Dark Current characteristics	Dark Current and Dark Current Fixed Pattern Noise for each layer	None	None
Dark Frame	Optical-Dark	Determine temporal and spatial non-uniformity	Read Noise and Read Fixed Pattern Noise	None	None
Responsivity	Optical - Bright	Determine response as a function of wavelength	Responsivity curves	Across detector response in 50nm bandwidths	None
Bright Field Measurements	Optical - Bright	Provides calibration and characterization of various FPA characteristics	Quantum yield, full well, linearity, and dynamic range	Dark to 1.5x full-well in all bands	None
Total Dose	TID	Measure radiation hardness of device.	0-100Krads with associated Dark and Optical Tests listed above	Each band	Logarithmic range of TID
Radiation response (dark)	Radiation	Determine pulse height distribution in each band. Will indicate effective active region sizes.	Mean pulse height Pulse height distribution	None	Several EPR values from 0.1-6/read
Pulse height Distribution	Radiation	Derive pulse height distributions	Pulse height distribution	None	<0.1 events/read
Correlated PHD	Mitigation	Derive statistics of ratios of pulses generated in layers	Pulse amplitude ratio statistics	None	<0.1 events/read
Mitigated Radiation Response	Mitigation	Test the effects of the mitigation method	Mitigated response	None	Several EPR values from .1-15/read

2.2   Measurement Of Optical Response.

We will now look at each of the optical characteristics of interest. These values were measured pre-radiation.

2.2.1   Dark Current.

Dark signal measurements as a function of integration time were made to determine the Dark Current. Note that for these measurements the read noise is removed through one-point subtraction of the mean dark frame. These were used to determine the Mean Dark Current (DCM). The results are shown in Figure 5.
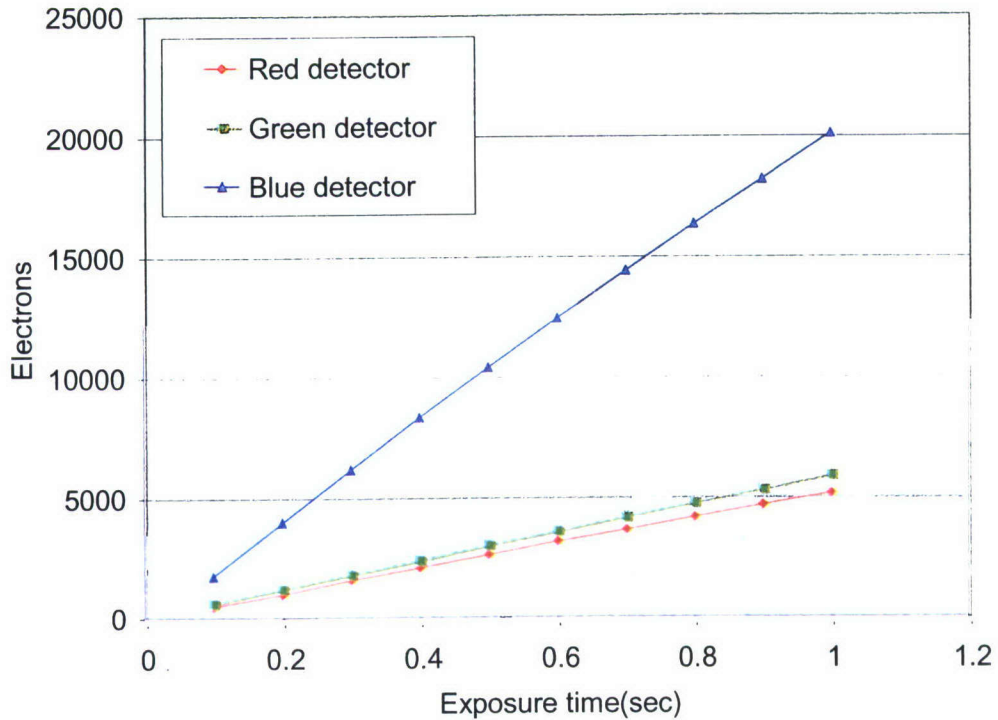
Figure 5.   **Slope of dark signal as function of integration time provides dark current.**

Fitting a line to these curves gave dark currents of 5234, 5904, and 20367 electrons/pixel/second or 1.0, 1.1, and 3.9nA/cm^2 for the red, green and blue layers, respectively. The higher value for the blue layer was not unexpected, as it is the topmost layer and unlike the underlying layers has the contribution of surface-states added to the sources of dark-current.

2.2.2   Dark Frame Measurements.

Dark Frame measurements were made to determine spatial and temporal noise. These measurements were taken without illumination and it is assumed for both of these quantities that measurements are taken in conditions such that dark current noise contributions are negligible. This measurement was performed with the built-in one-point subtraction routine (which uses a single dark frame as the reference) turned off. Instead the mean of the dark-frame set was used when correcting for the mean response of the device. The temporal noise, or Read Noise is defined as the standard deviation of the per-pixel value from frame-to-frame around the pixel mean. The pre-rad read-noise was about 114 +/- 8 electrons for the three layers.

The spatial noise or Read Fixed Pattern Noise (RFPN) is defined as the standard deviation of the mean per-pixel response versus the mean pixel response across the frame. This is ordinarily dominated by output amplifier threshold voltage variations. The pre-rad RFPN was approximately 650 electrons for the red and green layers and a bit higher, 790 electrons, for the blue layer. The one-point subtraction compensates for this effect even, as will be seen, when the amplifiers shift due to radiation-induced ionization.

Mean dark amplifier offset, i.e. the mean dark voltage value, was 27,000, 33,000, and 39,000 electrons for the red, green, and blue layers, respectively.

2.2.3 Responsivity And Bright Field Parameters.

Responsivity curves were produced for each detector layer, using 50 nm wideband-pass filters to select the stimulating light wavelength. Stimulating wavelength was varied by 50nm increments across the detector's sensitive waveband (from 405 to 660). These are shown in Figure 6 below. The low power scales are due to limitations of the light source at low wavelengths. It can be seen that for the shortest wavelengths the blue layer response dominates, and as the wavelength increases the green and then red layer response increases, with all layers responding approximately equally around 550 nm. These responsivity curves correlate to the overall manufacturer-provided frequency sensitivity curve shown in Figure 7.

From these curves we can derive a number of interesting characteristics. Using designed the trans-impedance of the detector, we see that a full-well of between $(86-93)*10^3$ electrons per layer, with a linear maximum full-well of about $(60-65)*10^3$ electrons (where non-linearity is chosen as that point at which the actual response varies from the linear fit by more than 5%). This corresponds to a dynamic range of about 790 or 58dB. Observing that the maximum response wavelengths for the blue, green, and red layers are 450, 550, and 650 nm, respectively, and taking into account the ¼ second integration time, we see maximum quantum efficiencies for each respective layer of roughly 26%, 17%, and 25%. The total absorption at these wavelengths for all three layers is roughly 37%, 44% and 46%, in good agreement with manufacturer specifications.
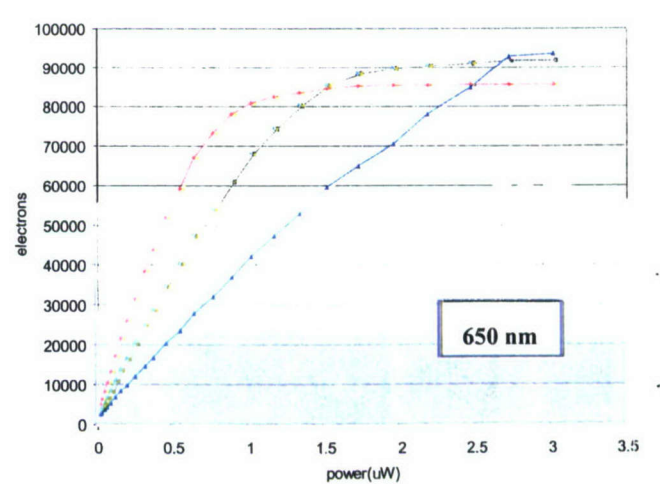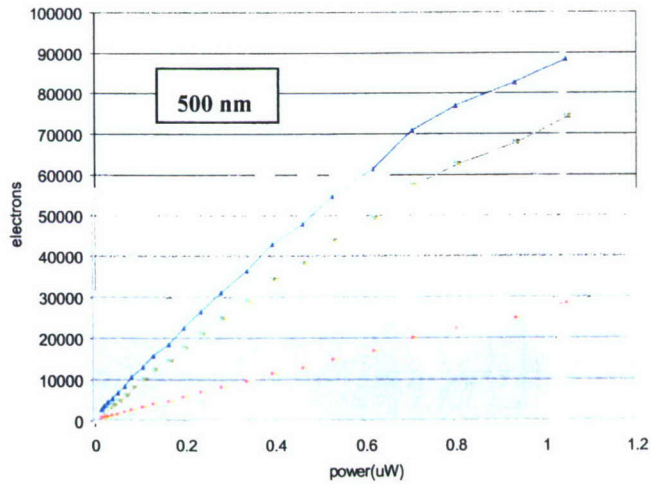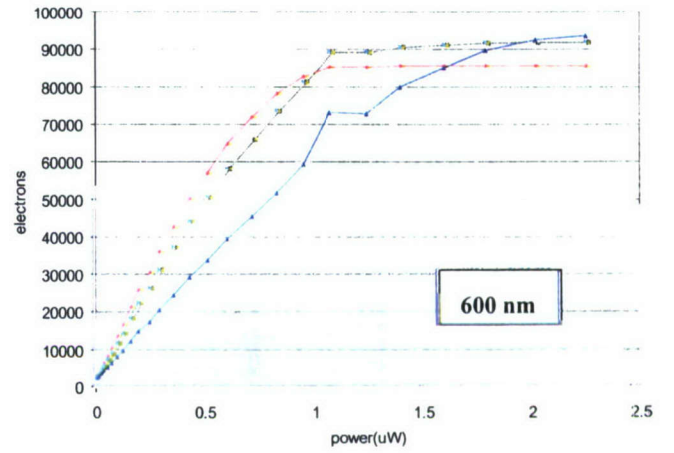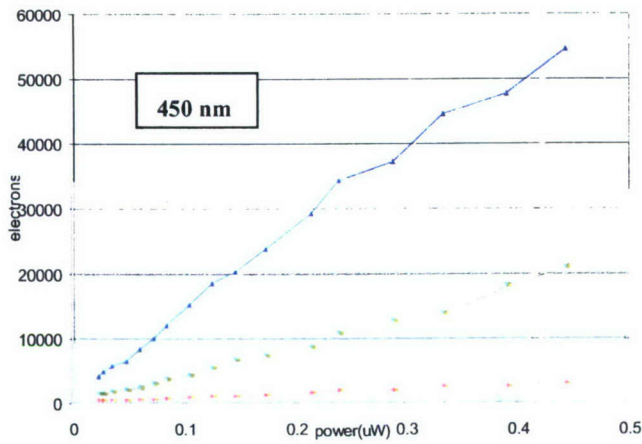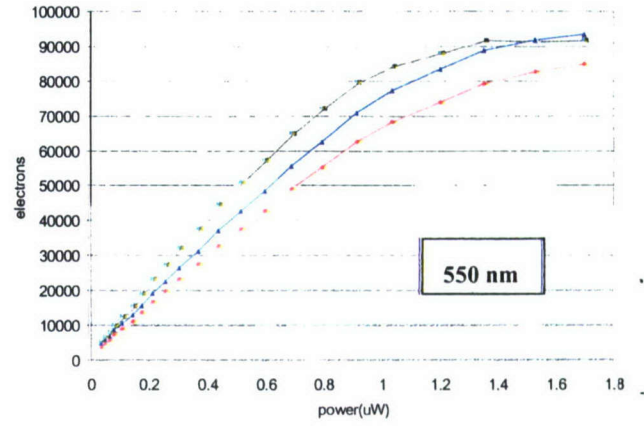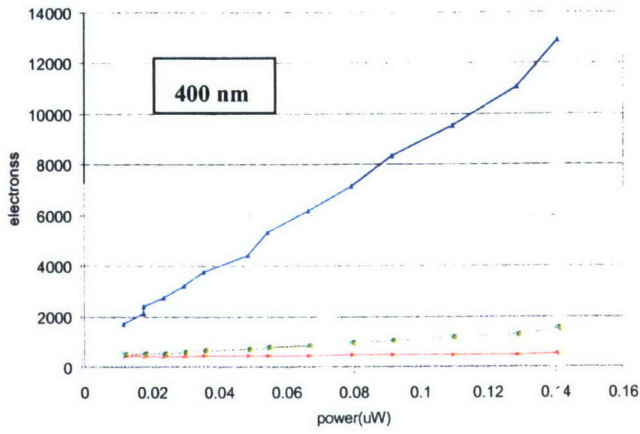
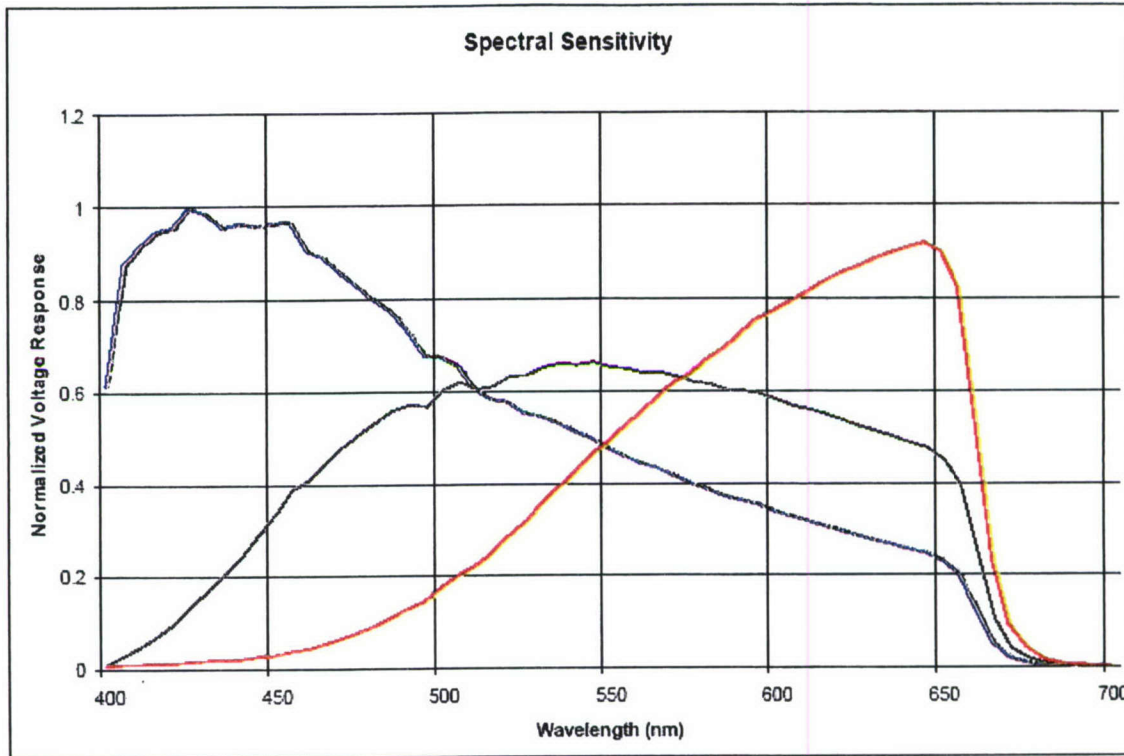**Figure 6.   Pre-radiation responsivity curves.**

Figure 7.   Typical spectral response curve (provided by Foveon).

2.3   Total Dose Testing.

Total Ionizing Dose (TID) testing was performed to determine the TID rad-hardness of the device. Optical characteristics were taken at logarithmically spaced TIDs. The results are presented below. The testing was stopped at 100KRads as a reasonable hardness level for such devices to reduce testing time even though the device was still operational.

2.3.1   Dark Current.

Dark current was calculated as is displayed in Figure 8. As can be seen, all three bands' dark current increased monotonically to approximately a factor of 3X at 100Krads. These final values are not prohibitively high for many applications. Further, these tests were performed at room temperature. Dark current decreases dramatically with temperature (a rule of thumb is a factor of 2 every 6 degrees Kelvin, or an order of magnitude for 20 degrees Kelvin) so even moderate cooling can bring the dark current down to desired levels.
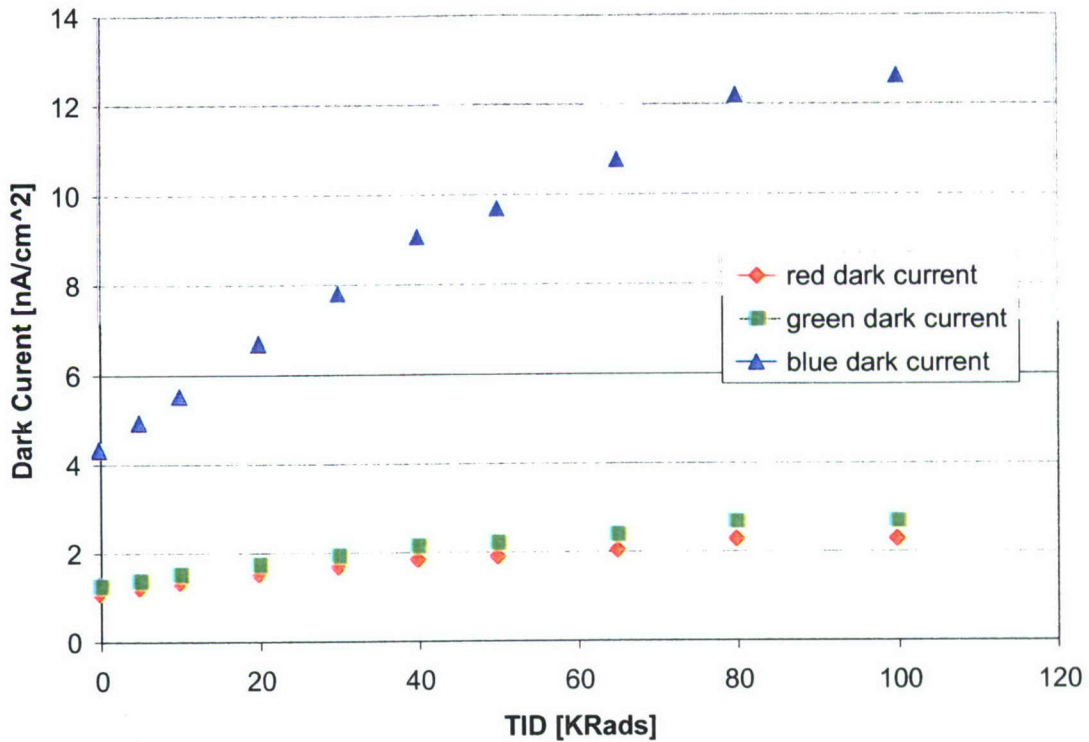
11

Figure 8.   Dark Current increases linearly to 3X at 100KRads.

2.3.2   Dark Frame Measurements.

2.3.2.1   Read Noise.

The read noise, as shown in Figure 9, was relatively unaffected by the radiation dose, showing only a slight increase. This increase is attributable to the increase in dark current. As can be seen in Figure 10, which shows the blue layer read noise for various sets of rows, the apparent read noise seems to increase with row number. Because the rows are read out sequentially, the later rows necessarily accumulate more dark current, which for higher dose becomes non-negligible compared to the read noise (Note that the lower row numbers 100-199 are used in the graph of read noise, Figure 9, to reduce this effect).
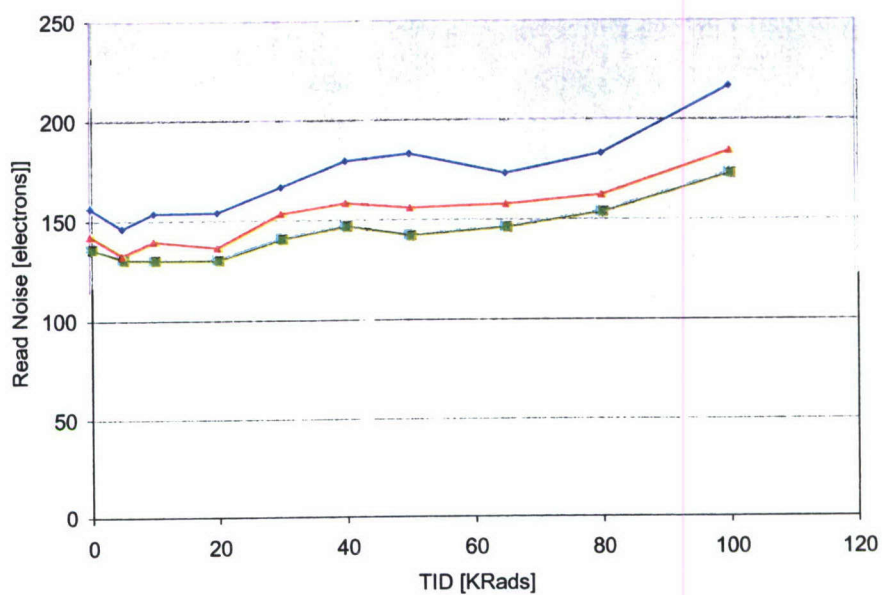
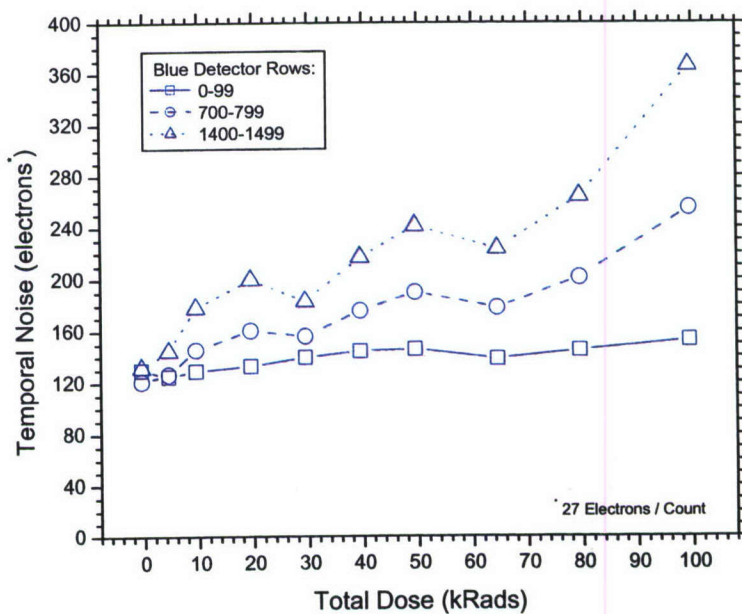**Figure 9.** Read noise unaffected by radiation dose (rows 100-199 shown).

Figure 10. Read noise for various sets of rows as function of total dose (blue layer) show effect of increased dark current.

2.3.2.2 **Read Fixed Pattern Noise (RFPN).** RFPN increased slightly with TID (note the limited y-scale in Figure 11). As will be discussed in the next section, the dark amplifier offset, i.e. the dark frame uncorrected pixel value, was affected by the TID, and as RFPN is very dependent on variations in this offset, an increase in this term is not unexpected. This variation was easily compensated for by the 1-point correction.
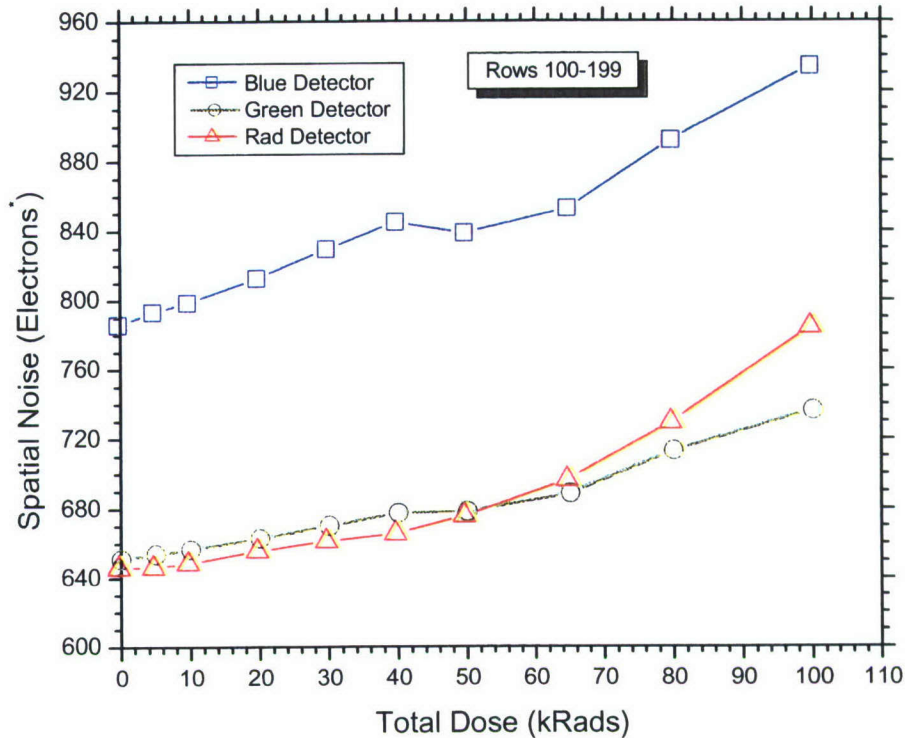

Figure 11.   Slight increase in RFPN with Total Dose.

2.3.3   Responsivity and bright field parameters.

Responsivity curves for the three layers are shown in Figure 12 to Figure 14. Two frames were taken at each illumination level, with a 0.25 second integration time. This data was taken, as before, using a 1-point dark correction frame taken at each TID level. Except for a slight reduction in amplification for the blue layer at the highest TIDs, the responsivity is essentially unchanged up to 100KRads, as are the associated bright field parameters. Graphing the mean dark pixel offset (i.e. the mean pixel value of the 1-point dark correction frame) as shown in Figure 15, we see that there is, in fact, a TID effect in that the mean dark pixel offset increases approximately linearly with dose. With this corrected, TID effects up to 100KRads can be almost completely masked for this technology, making this a promising device for high radiation environments.
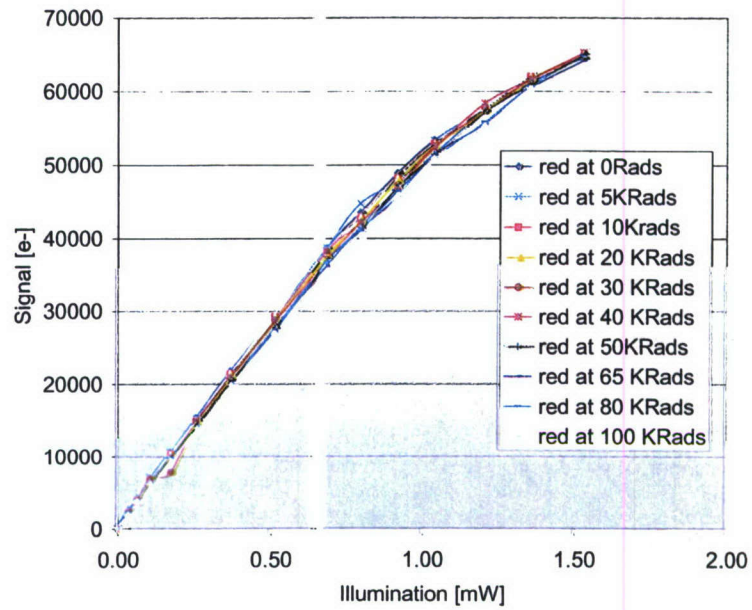
14

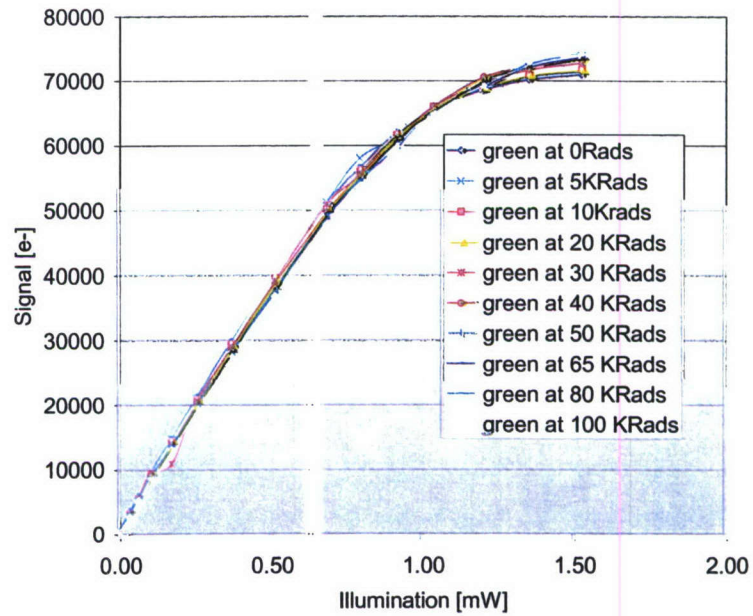**Figure 12.** Red respon sivity for various TID: unchanged.

Figure 13. Green respo isivity for various TID: unchanged.
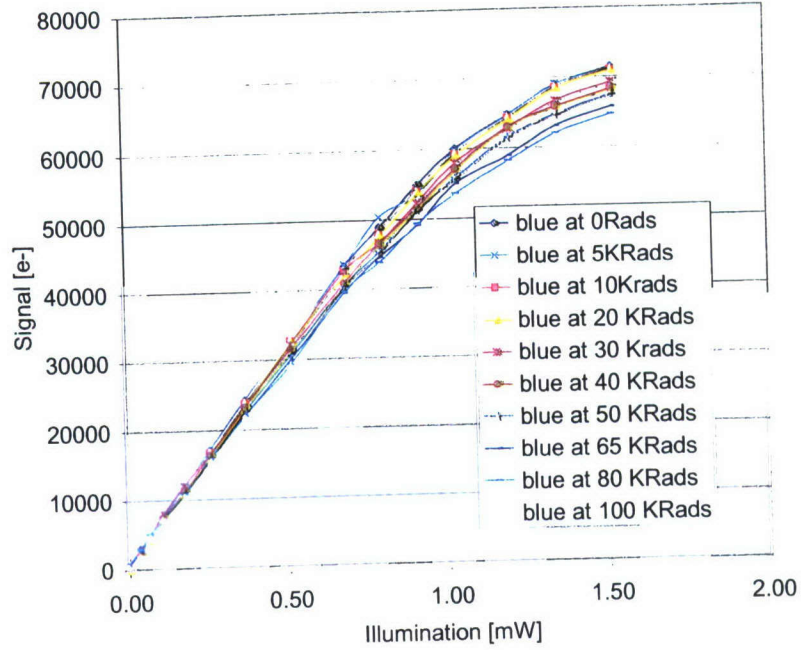
Figure 14. Blue responsivity for various TID: slight loss of responsivity at high dose.
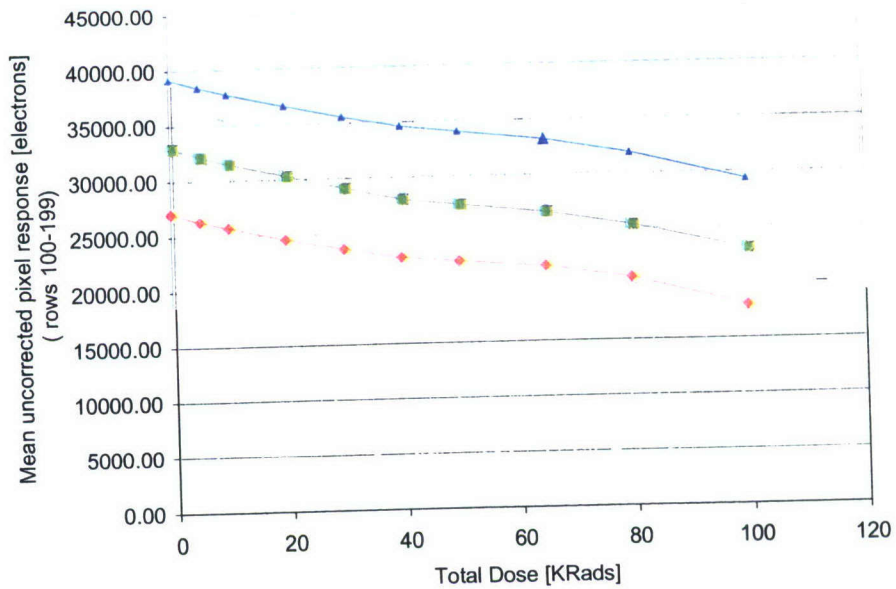

Figure 15. Mean pixel response w/o 1-pt correction as function of total dose shows effect of TID induced voltage offset.

2.4   Measurement Of Transient Radiation Response.

Measurements of the radiation response of each layer due to gammas were made using the 870Ci ^{137}Cs source at ATK-MR Longmire Laboratory. Event rates in the 0-10 events/read range were used. Low event rate data (< 0.1 events/read) were taken to provide statistics of the pulse height distribution curves for the individual layers as well as for the device as a whole.

The distribution of the ratios of the pulse heights generated in each layer of the pixel relative to the others was derived in order to determine the best way to correlate the signal generated in the individual layers, and how to best remove the response. This also measured the degree of "mis-fit" between the layer responses, which will be the ultimate limit on the efficacy of this mitigation method.

It should be noted that the data acquired lacked the lowest order bit. This was due to programmed-in data processing that the manufacturer was unable to correct before testing was performed. This reduction in quantization accuracy made it difficult to obtain good transient data from the thinnest layer (blue) which has the lowest radiation response.

2.4.1   Mean Pulse Height, PH.

The mean response to a gamma event, the so-called pulse height, PH, was determined by taking advantage of the finite time required to read a row of the FPA. Under the operation of the Foveon device, the voltage created by the measured charges in the pixels of a given row is copied to a holding row, and each pixel row is read out. This forms, in effect, a snapshot of each row at the time the copy was made. As the device continues to accumulate charge during the read, each row is in effect exposed to a different event rate, characterized by $D*r_i/R$; where D is the total number of events per pixel over the time of the read, r_i is the number of the row in question, and R is the total number of rows.

Plots of the response vs. this event rate (where the rows were viewed in bins of 100 for convenience) for the red and green layers are shown in Figure 16 and Figure 17. Values under 300 electrons are in the non-linear region of the device and the fit was therefore made above this value. Photon transfer curves were produced for the red and green layers to obtain a good measurement of the electrons/count response in this low response region, giving values of 5.95 and 8.27 for the green and red amplifiers, respectively. Using these values, a fit of the slope in the linear region of the graphs then provides the mean pulse height/event, corresponding to 629 electrons for the red layer and 159 for the green layer. These were in very good agreement with predictions based on simple parallelepipeds which predicted values of 575 electrons for the red and 143 electrons for the green layers.

The mean pulse height for the blue layer was very small, as expected, and was in the noise even for the largest EPR. Based on the other layers and our calculations, we expect the mean pulse height to be approximately 60 electrons.
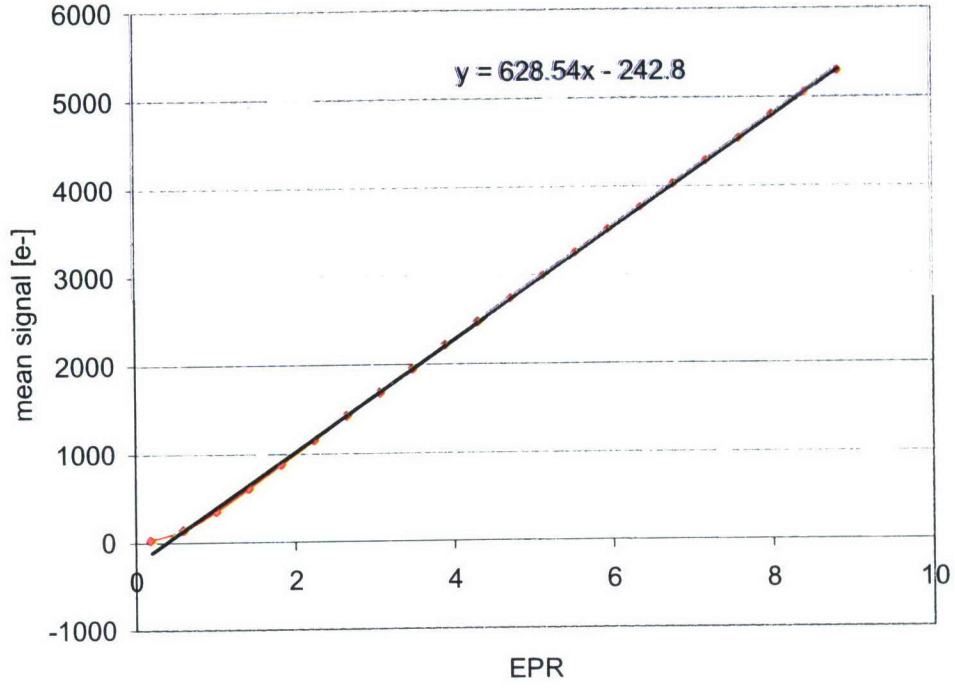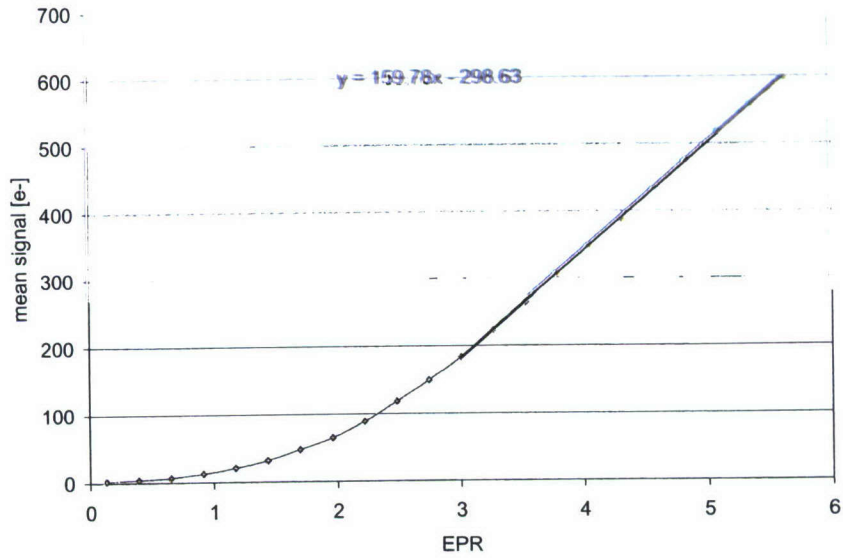
17

Figure 16. Red response as a function of event rate.

Figure 17. Green response as a function of event rate.

Section 3
SRTS mitigation

Transient radiation-induced noise in Focal Plane Arrays (FPAs) is of growing importance as sensors are designed for increasingly taxing radiation environments. It is not sufficient that a detector survive the radiation dose; the sensor must be able to operate in the presence of radiation-induced noise to adequate levels to fulfill its mission. In the past, shielding and off-chip signal processing were able to mitigate the radiation effects. As mission environments become more challenging this is no longer the case, and in-pixel or on-FPA mitigation techniques become essential (See Figure 18).
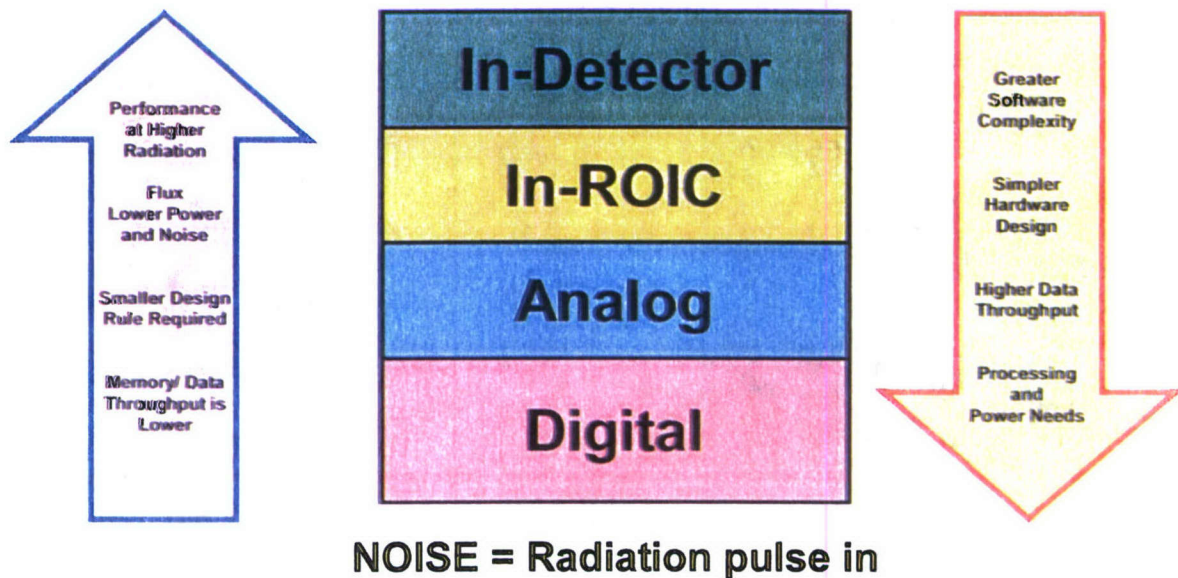

Performance at Higher Radiation	In-Detector	Greater Software Complexity
Flux Lower Power and Noise	In-ROIC	Simpler Hardware Design
Smaller Design Rule Required	Analog	Higher Data Throughput
Memory/ Data Throughput is Lower	Digital	Processing and Power Needs

NOISE = Radiation pulse in

Figure 18.   Trade-offs in radiation mitigation.

In earlier analysis of various mitigation methods (Doughty, to be published) (Goldflam, to be published) one stood out as of particular interest: Self-Referential Transient Suppression (SRTS). This design was seen to mitigate mean-to-low radiation pulses that are smaller than the noise of the system (a noise source that is inaccessible to mitigation methods that depend on "recognizing" the noise event, and which provide the bulk of the radiation noise under current mitigation approaches). Preliminary modeling indicated that it also would perform well at mitigating large noise events. While the largest pulses still remain, including large negative pulses that are a characteristic of this mitigation method, these few large pulses can be eliminated later in the processing chain using known methods. This mitigation method could therefore be a very promising one for the most challenging radiation environments.

Self-Referential Transient Suppression (SRTS) is defined as two detectors, the first being optically active and subject to radiation-induced noise spikes, the second (the mitigating detector), directly under the first, being optically inactive but still sensitive to radiation-induced noise events. As a radiation particle travels through a semi-conductor device, there is a probability that it will interact with the material, producing Compton electrons that donate energy to creating electron-hole carrier pairs. These carriers are indistinguishable in type from those that are created by photon generation and constitute the dominant noise source due to radiation in FPAs. The carriers are generated along a line traveling through the detector. The signal induced in a device is essentially linearly dependent on the distance the particle travels through the device (barring changes in energy deposition rates as the particle loses energy along the path). The alignment of the two detectors insures that the path-lengths in each will be similar, except in cases where the particle exits or enters an edge (see Figure 19).
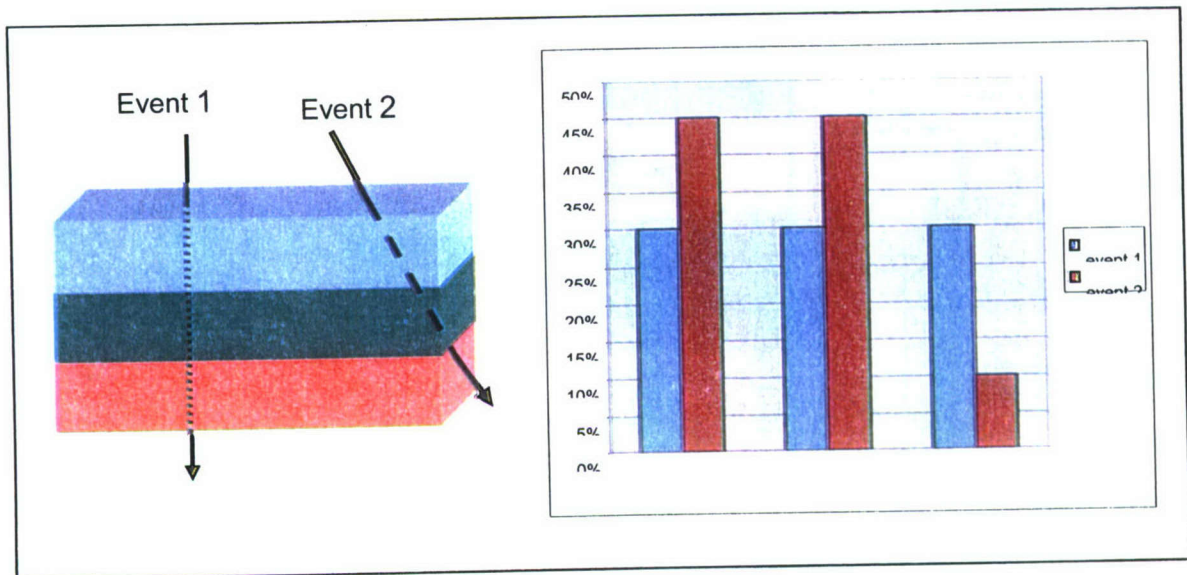

Figure 19.   Radiation induced pulse height in each layer depends on radiation path.

While for a device that is thin relative to its other dimensions, the path ratios are more likely to be like those shown in event 1 than for event 2, the statistical mismatch between the pulses in each layer is a dominate limitation on this mitigation approach.

The structure of the Foveon device obviously lends itself to this kind of mitigation. It should be pointed out that the Foveon layer structure as it stands is not optimized for STRS, although the modifications would be straightforward. In this study we are comparing the mitigation achievable with the commercial Foveon device to that predicted for the current layer structure to show the feasibility of the approach and to verify the model. Optimization will be the next step.

3.1 Modeling Algorithm.

To obtain a prediction of the expected efficacy of the mitigation with the commercial layer structure, a simulation of the Foveon device was performed using the following algorithm:

- Each sample result from the model represents the radiation-induced signal from a single read of the detector pixel. For each sample, the mean EPR is used to draw from a Poisson distribution to generate the number of events for the two radiation types. Then for each event, the following computations are performed:

- A random particle direction is chosen to simulate omni-directional flux. More extensive modeling could take into account the directional shielding, but for this study a homogeneous flux was used.

- Chord length through two layers is determined.

- An energy is randomly chosen from an appropriate energy spectrum.

- Energy deposited along the particle track is computed, taking into account the change in energy deposition rate (dE/dx) along track. For gamma/betas the energy deposited is relatively insensitive to particle energy, but this will be a more important effect should protons or heavier particles be used.

- The resulting carrier generation is computed based on material characteristics (silicon, in this case).

- The mitigation signal is subtracted from the sensor signal to determine noise signal. The subtraction is weighted by the ratio of the thicknesses to provide best cancellation for those paths that travel from top to bottom of the stack, as to first order the signal is proportional to the path-length (see Figure 20). For the actual device this ratio, α, was optimized for the radiation range of interest.
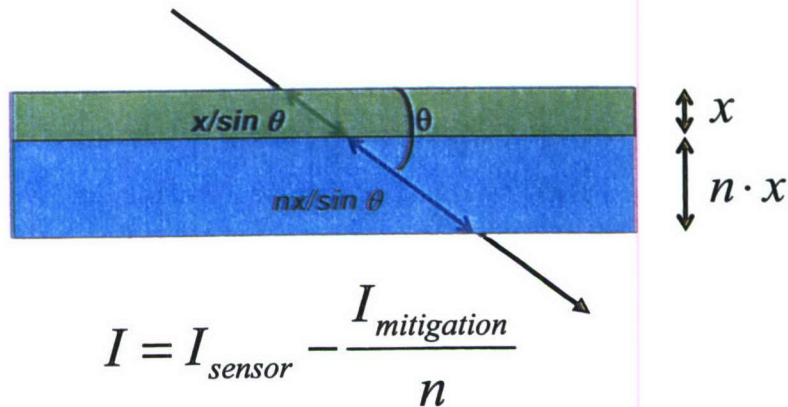
$$I = I_{sensor} - \frac{I_{mitigation}}{n}$$

Figure 20.   Relation of top-to-bottom pathlengths.

3.2 Mitigation Test Results.

To examine the statistics for the Foveon device, event rate data (ranging between 0.1 and 6 events per read) was taken to measure the statistics of the relative pulse sizes from each layer of a pixel experiencing an event. This allowed us to determine the accuracy of the mitigation that can be achieved with the Foveon pixel.

Using the red and green bands as mitigation layers for each other, the value of α, the ratio used for correction of the two signals, was varied to optimize the noise of the detection layer. An example optimization for green-corrected-with-red is shown in Figure 21, with the optimum α, in this case, being equal to 1.78.
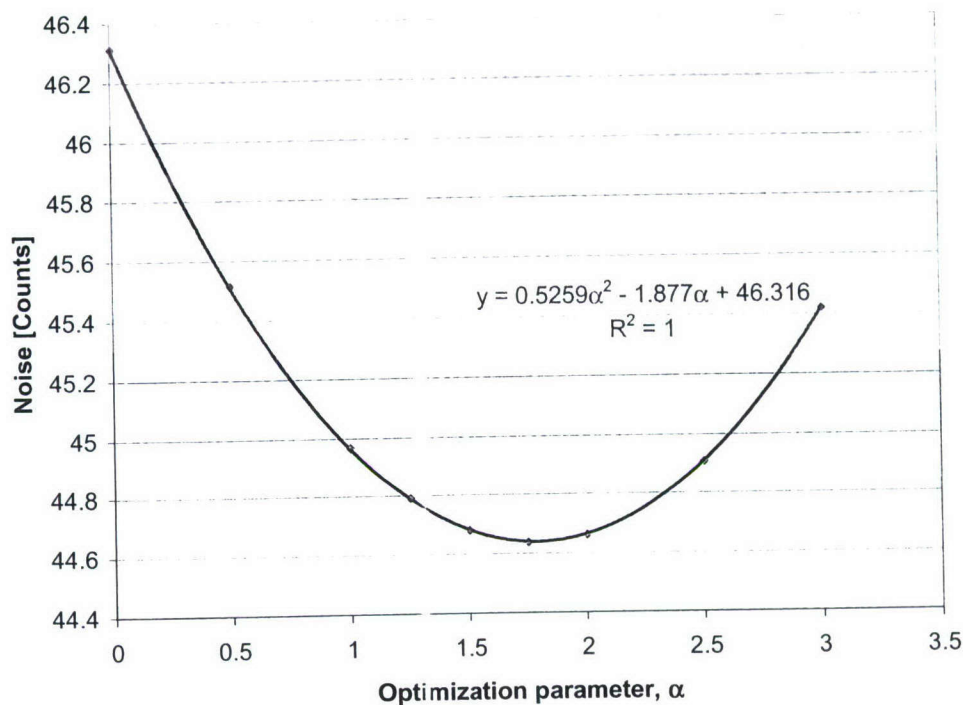

The plot shows Noise [Counts] on the y-axis versus Optimization parameter, α, on the x-axis, with the fitted curve:

$$y = 0.5259\alpha^2 - 1.877\alpha + 46.316$$
$$R^2 = 1$$

Figure 21.   Noise under 1.4 event/read irradiation as a function of correction ratio, α.

3.2.1   Comparison Of Predicted vs. Actual Result.

The simulated mitigated and unmitigated histograms for red-corrected green detection under 6 events per read irradiation are shown in Figure 22. A plot of the measured data used for mitigation of the green layer is shown in Figure 23 (the second peak in the unmitigated histogram is an artifact due to the missing bit). As can be seen, there is good agreement in the form of the predicted and actual data.
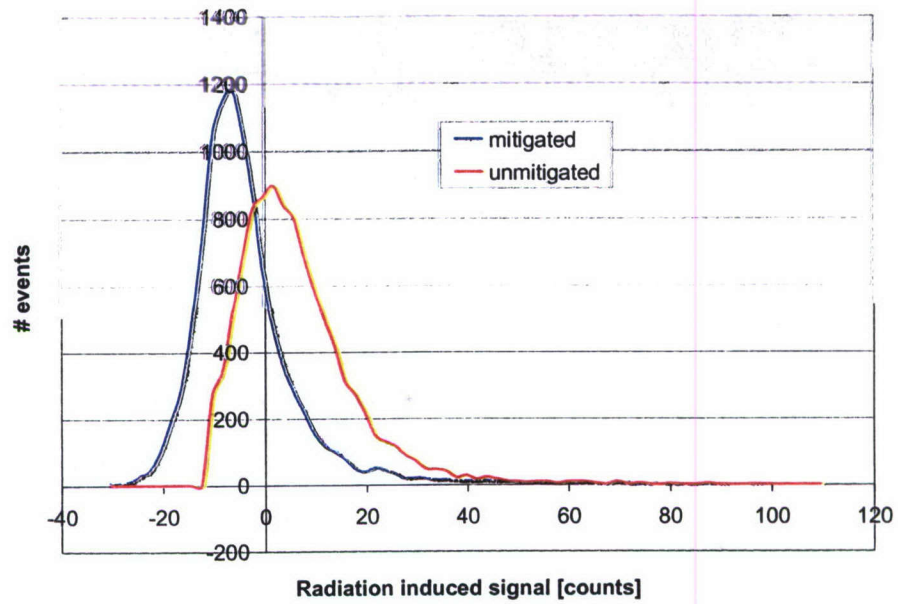
22

Figure 22. Simulated red-corrected green mitigated and unmitigated response: 6 events/read.
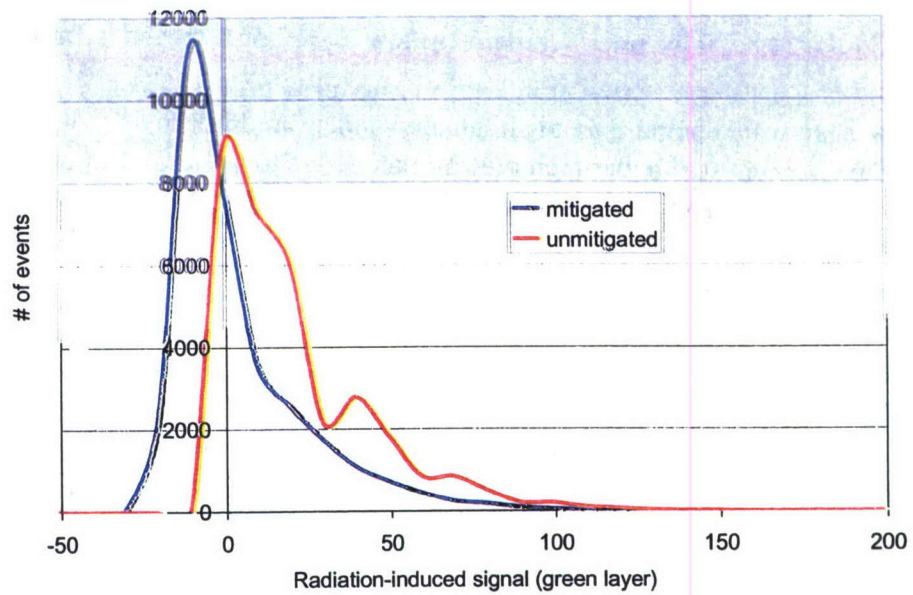

Figure 23. Measured red-corrected green mitigated and unmitigated response: 6 events/read.
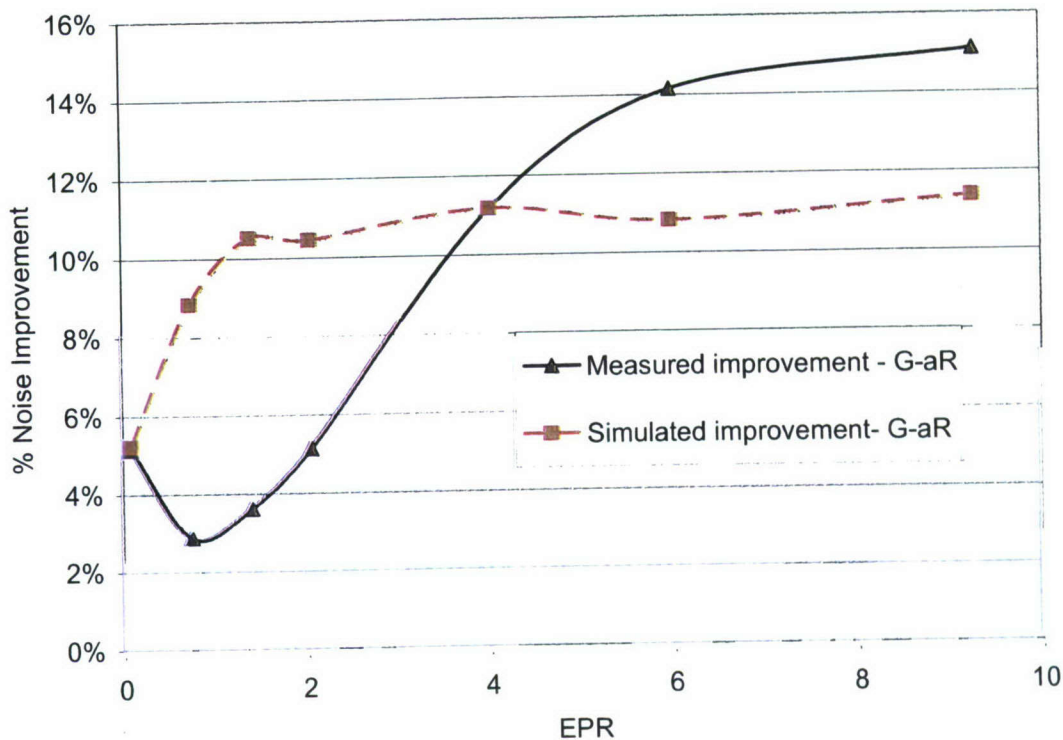
Figure 24.   Noise improvement for simulated and measured mitigation.

In Figure 24 is shown a comparison of simulated vs measured improvement. Note that the measured improvement was better than the simulated, due to the ability to optimize α, the matching parameters. Again, this particular thickness matching was not optimized. Mitigation depends on the geometry of the device as well as, to a lesser extent for gamma/betas, the energy of the expected radiation.

As the current device is not optimized, a simulation study was done of mitigation vs. layer thickness. A differentiated histogram of the result of mitigation for a range of geometry ratios is shown in Figure 25. As can be seen, a thinner mitigation layer provides the best mitigation, with a 0.15 micron mitigation layer extending the effect of excellent mitigation to 60% of the events, with good mitigation for an additional 25 %. The final 15% of the events are large and can be mitigated using known techniques for removal of large radiations events, as shown schematically in Figure 26.
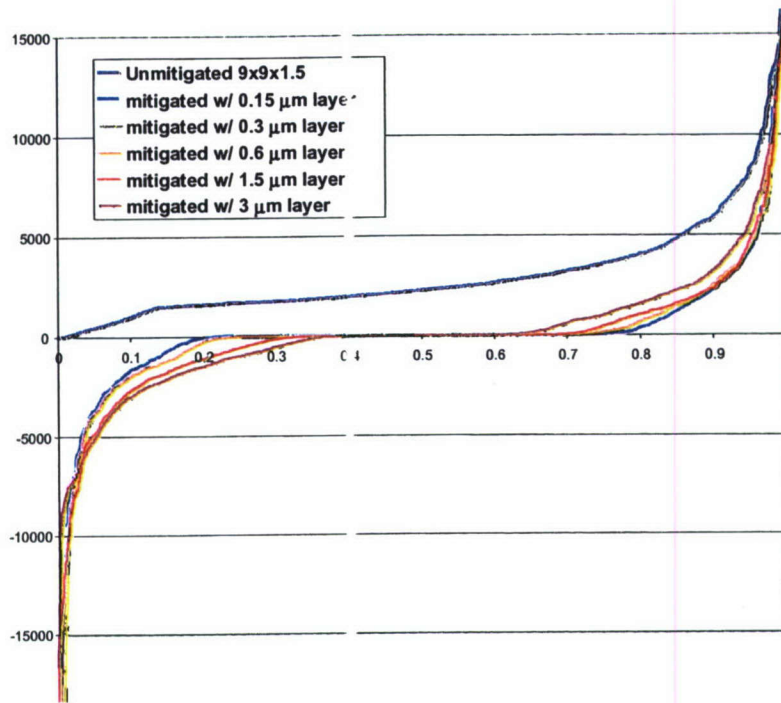
Figure 25. Simulated SRTS mitigation for detector layers of different thicknesses shows thin layers provided best mitigation
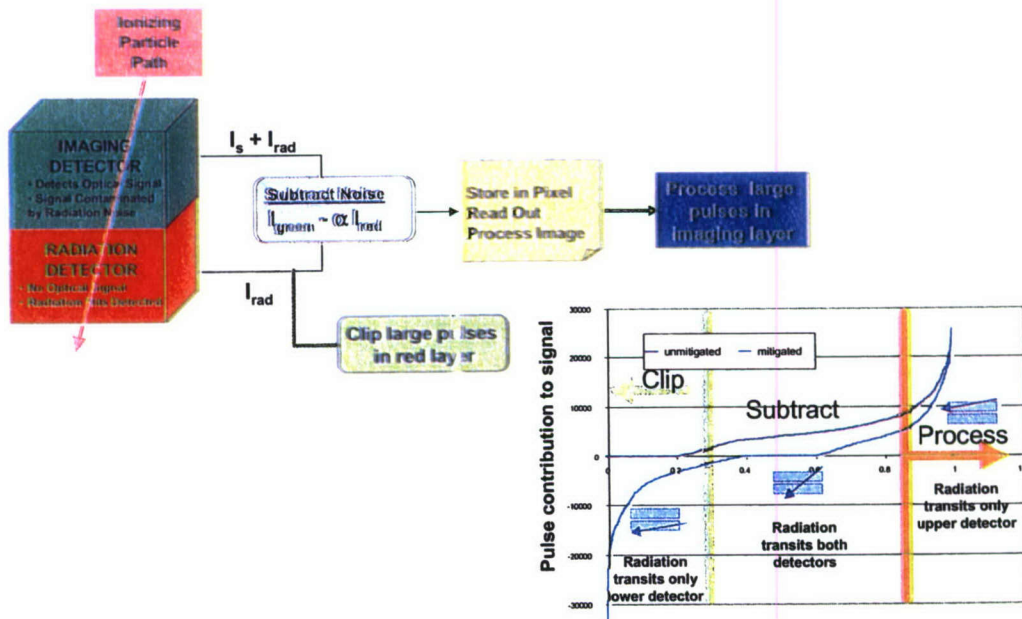

Figure 26. Optimization scheme for removal of small and large radiation events.

Section 4
Next Steps

Having tested the Foveon device (and taking into account the specifics of device dimensions and their effect on the matching between the optical and mitigation layers), a good understanding of the efficacy of the SRTS method has been achieved. Further, as the Foveon device proved to have inherent rad-hardness there will, no doubt, be many applications for which it could be used at considerable savings in cost and development time. Secondly, and of particular interest to programs wanting a device to operate in challenging radiation environments, versions of the SRTS method can then be combined with other mitigation methods to provide a device that is extremely resistant to radiation noise. Foveon representatives have expressed the company's willingness to license the method for use in other technologies, which would allow for the development of such custom devices as well as expanding its use into other materials and wavebands, including multicolor devices. It should be noted that SRTS applies even for small pulse-height radiation contamination (unlike such methods as sub-framing and continuous suppression, which require a radiation contamination to be of a certain magnitude before it can be detected and removed). It is, therefore, a good fit for further mitigation of a thinned device, for which the mean pulse height has been greatly reduced. This combination of the two mitigation methods shows promise of providing a self-mitigating visible detector particularly suitable for use in high radiation environments.

Section 5
References

Doughty, K., R. Goldflam, "Effects of Radiation Noise and Mitigation Techniques on Location and Identification of Targets", JRERE 2003, to be published.

Goldflam, R., K. Doughty, Tostanoski, M., "Modeling of radiation-induced noise in-pixel suppression techniques", JRERE 2002, to be published.

DEPARTMENT OF DEFENSE

DEFENSE TECHNICAL
INFORMATION CENTER
8725 JOHN J. KINGMAN ROAD,
SUITE 0944
FT. BELVOIR, VA 22060-6201
2 CYS   ATTN: DTIC/OCA

ITT INDUSTRIES
ITT SYSTEMS CORPORATION
1680 TEXAS STREET, SE
KIRTLAND AFB, NM 87117-5669
2 CYS   ATTN: DTRIAC

DEFENSE THREAT REDUCTION
AGENCY
8725 JOHN J. KINGMAN ROAD
STOP 6201
FT. BELVOIR, VA 22060-6201
2 CYS   ATTN: RD/L. PALKUTI

DEPARTMENT OF DEFENSE CONTRACTORS

ATK MISSION RESEARCH
1300 NORTH 17TH STREET
735 STATE STREET
P.O. BOX 719
SANTA BARBARA, CA 93101
        ATTN: K. DOUGHTY